PNAS
www.pnas.org

Supplementary Information for

# Mesoscale Bicontinuous Networks in Self-healing Hydrogels Delay Fatigue Fracture

Xueyu Li, Kunpeng Cui, Tao Lin Sun, Lingpu Meng, Chengtao Yu, Liangbin Li, Costantino Creton, Takayuki Kurokawa, and Jian Ping Gong*

*Jian Ping Gong

Email: gong@sci.hokudai.ac.jp

**This PDF file includes:**

Supplementary text

Figs S1 to S11

SI References



www.pnas.org/cgi/doi/10.1073/pnas.2000189117

**Supplementary Information Text**

## Methods

**Preparation of polyampholyte hydrogels (PA gels).** Polyampholyte hydrogels (PA gels) were synthesized by a one-step random copolymerization of precursor aqueous solution containing anionic monomer sodium p-styrenesulfonate (NaSS), cationic monomer methyl chloride quarternised *N*,*N*-dimethylamino ethylacrylate (DMAEA-Q), UV initiator α-ketoglutaric acid, and chemical cross-linker N,N-methylenebis(acrylamide) (MBAA) (the structures are presented in **Fig. S1**) according to refs (1-3). The total monomer concentration $C_m$ is 2.0 M with monomer ratio of NaSS:DMAEA-Q=0.515:0.485, and both of the UV initiator and cross-linker content are 0.1 mol% (relative to $C_m$) in the precursor solution. The precursor solution was degassed and then injected into a reaction cell (20 cm×20 cm) consisting of a pair of parallel glass plates separated by a silicone spacer with thickness of 2 mm in argon atmosphere. Polymerization was carried out in argon atmosphere keeping the oxygen concentration less than 0.1 ppm by irradiating UV light (wavelength 365 nm, light intensity ~4mWcm$^{-2}$) from both sides of the reaction cell for 11 h. After polymerization, the as-prepared gels were taken out and immersed in de-ionized water to dialyze the counter-ions and to reach equilibrium. To tune the bicontinuous hard/soft phase networks, the as prepared gels in the same batch were dialyzed in water with temperature $T_{dial}$=5, 30 and 60 ℃, respectively. The dialyzed samples contain no small counter-ions. After dialysis, gels were stored at room temperature before use. The gels shrink to ~1.64 mm in thickness after dialysis, denoted as PA-$T_{dial}$.

**Water content**. The water content of the gels $c_w$ (wt%) was measured using the moisture balance (Moisture Balance; MOC-120H, Shimadzu Co.), where the weight change of samples was monitored during the drying process. The $c_w$ are 0.461±0.41, 0.455±0.13 and 0.455±0.23 for PA-5, PA-30 and PA-60, respectively.

**Tensile tests.** The tensile tests were carried out on dumbbell shaped samples with the standard JIS-K6251-7 size 12 mm in gauge length ($L_0$) × 2 mm in width ($w_0$) using an INSTRON 5566 universal tensile tester. To prevent water from evaporating from the samples, the dialyzed sample were tested under constant moisture environment. A constant velocity $v$=10 mm/s was applied during the stretching. The nominal stress was obtained from the tensile force divided by the initial cross-sectional area of the sample and the elongation ratio λ was obtained from the ratio of the stretching length $L$ and the initial length $L_0$.

**Fatigue experiments.** Fatigue experiments were performed on a tensile tester (Shimadzu Autograph AG-X tensile machine) with a 100 N load cell. Two different samples with pure shear geometry (10×50×1.64 $mm^3$, $H_0 \times L_0 \times t$), single-edge notched and unnotched, were used. To prevent samples from dehydrating, a humidity chamber was set on the tensile tester. Water vapor was sustainably supplied in the chamber during the test (**Fig. S2*A***). Cyclic loading-unloading was performed along the $H_0$ direction at a nominal strain rate of 1 $s^{-1}$ with the maximum elongation ratio in each cycle held at $\lambda_{max}$, while the minimum held at λ=1. The test temperature was kept constant at 24 ℃. A digital camera (canon 7D) was used to record photos during crack extension for notched samples every 5 min. The resolution of this optical method is 10 μm. The length of crack extension during cyclic loads was recorded as $c$. To improve the reliability of results, fatigue tests

were performed at least twice for several representative values of $\lambda_{max}$. The amplitude of load in terms of the energy release rate $G$ was calculated from

$$G = W_e(\lambda_{max})H_0 \qquad \text{(S1)}$$

where $H_0$ is the initial distance between the two clamps, $W_e(\lambda_{max})$ is the elastic strain energy density of the unnotched sample at steady state. Softening and shakedown were observed during cyclic loading for unnotched sample. After 3000 cycles, the cycle approaches steady state (**Fig. S2 *B* and *C***). At steady state, gels still exhibit a large hysteresis loop, caused by the fast dissociation and reassociation of weak ionic bonds (**Fig. S2*D***), which contribute to the nominal fracture energy $\Gamma$. Here, to obtain the intrinsic fracture energy, the hysteresis energy was excluded. Thus, the integral area under the unloading curve $W_e(\lambda_{max})$ at the 3000$^{th}$ cycle was used to calculate $G$.

The fatigue threshold predicted by Lake-Thomas model(4, 5) $\Gamma_0 = \Sigma U_{c\text{-}c} N_e$ is ~24 J/m$^2$ for the PA gels with different $T_{dial}$ applied in this work, where, $\Sigma$ is areal density of chains crossing the interface (~2.24×10$^{16}$ /m$^2$), $U_{c\text{-}c}$ is the energy stored per C-C bond (347 kJ mol$^{-1}$), $N_e$ is the average number of bonds per polymer strand (~2000 bonds between two crosslinks)

**In-situ SAXS measurements during stretching.** The evolution of bicontinuous phase structure in PA gels during stretching was characterized by *in-situ* small-angle X-ray scattering (SAXS), which was carried out at the Shanghai Synchrotron Radiation Facility (BL19U2, Shanghai, China). The X-ray wavelength is 1.03 Å. A two-dimensional detector (Pilatus 1M with a resolution of 981×1043 pixels and pixel size of 172 μm,

Dectris Co. Ltd) was used to record data. The sample-to-detector distance was 5730 mm. A tensile machine with well controlled humidity and temperature (Hefei Puliang Technology Co., Ltd) was used to perform uniaxial tensile and cyclic loading experiments. The nominal loading strain rate was controlled to be 1 $s^{-1}$. Experimental temperature is 24 ℃. 2D SAXS patterns were acquired at a rate of 0.25 s/frame. The resulting strain, stress and SAXS patterns were recorded.

The *in-situ* SAXS experiments were performed on samples with a tensile strip geometry. As the bicontinuous phase networks of PA gels has a large phase mesh size $d_0$, the scattering signal parallel to deformation direction exceeds the detecting range at large $\lambda_{max}$. To obtain the microscopic structural information under stretch, the signal from the direction perpendicular to the stretch direction had to be used. For a pure shear geometry(6, 7), the affine deformation follows $\lambda_1=\lambda$( parallel to stretching direction), $\lambda_2=1$ (sample width direction), $\lambda_3=1/\lambda$ (sample thickness direction), since the gels are incompressible. Therefore, no deformation occurs in the width direction perpendicular to the stretching. Furthermore, SAXS could not measure the structural change in the thickness direction to obtain $\lambda_3$. Thus, instead of pure shear geometry, we used gels with a strip geometry (16×7.5×1.64 $mm^3$, **Fig. S3*A***), which should follow $\lambda_1=\lambda$, $\lambda_2=\lambda_3=1/\sqrt{\lambda}$ for affine deformation. The deformation of the phase mesh size $d_\perp$ in the perpendicular direction was detected until the fracture of the sample (**Fig. S3 *C* and *E***).

The evolution of SAXS patterns during tensile test for the representative gels PA-5 and PA-60 are presented in **Fig. S3*C***. The initial scattering intensity of PA-60 is much stronger than that of PA-5, indicating a stronger phase contrast. The undeformed gels show an isotropic ring on the 2D SAXS pattern. It converts into an ellipse with its major

axis being perpendicular to the stretching direction with increasing λ, suggesting an elongation of the phase structures in the stretching direction. The scattering signal in the stretching direction gradually moves toward the beam stop with increasing λ and exceeds the detectable range after λ=1.8, while the signal in the perpendicular direction moves away from the beam center with increasing λ, and finally converts to two slender intense spots (**Fig. S3*C***). These results indicate the formation of highly oriented structure along the stretching direction.

To investigate the effect of the bicontinuous phase networks on the fatigue-resistance behavior, *in-situ* time-resolved SAXS experiments were performed to observe the evolution of the structure under cyclic tensile deformation using samples with geometry in **Fig.S3*A*.** PA-5 was chosen as a representative. Samples are subjected to cyclic loading for 1000 cycles at $\lambda_{max}$=2.54 ($<\lambda_{affine}$) and $\lambda_{max}$=3.44 ($>\lambda_{affine}$) under nominal loading strain rate 1 $s^{-1}$. The SAXS data were collected at the 1$^{st}$, 3$^{rd}$, 300$^{th}$ and 1000$^{th}$ cycles.

Fit 2D software from the European Synchrotron Radiation Facility was used to analyze SAXS data. The background scattering from the air and water was subtracted from the data. The 2D SAXS patterns were integrated along the azimuthal direction to obtain 1D scattering profiles as a function of the scattering vector

$$q = 4\pi\left(sin\ \theta\right)/\ \lambda \qquad \text{(S2)}$$

where $q$ is the module of scattering vector, $2\theta$ the scattering angle, and λ the X-ray wavelength. The spacing between adjacent hard (soft) phases (phase network mesh size, $d$) was obtained from the position of the scattering maxima $q_{max}$ according to Bragg's law

$$d = 2\pi / q_{max} \qquad \text{(S3)}$$

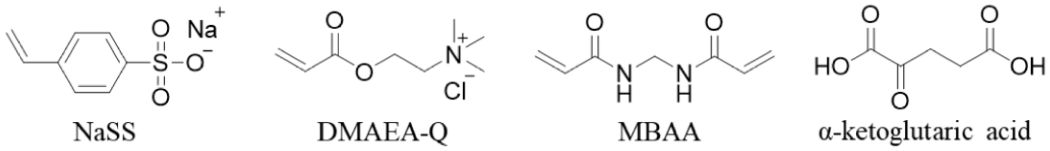


**Fig. S1.**

**Chemical structures of molecules used in this work**: anionic monomer NaSS, cationic monomer DMAEA-Q, chemical cross-linker MBAA and UV initiator α-ketoglutaric acid.

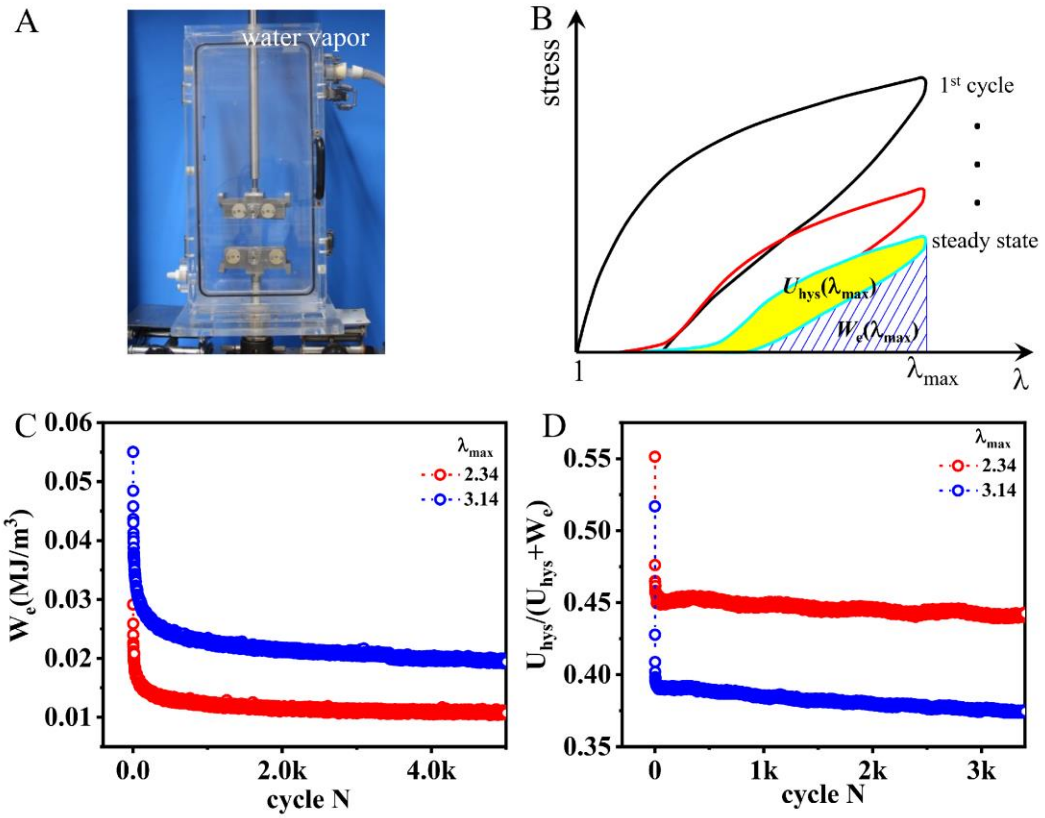


**Fig. S2.**

**Experimental setup for fatigue test and method to obtain energy release rate *G*.** (***A***) Photo image of the experimental setup with continuous humidification to prevent hydrogel drying. Before and after the fatigue test, the weight of gel changes less than 2%. (***B***) Scheme of loading-unloading curves to $\lambda_{max}$ with increasing cycle *N*. The curves drop greatly at the beginning of the cycles and reach a steady state after thousands of cycles. The hysteresis loop shown by the yellow color presents the energy density dissipated during deformation $U_{hys}(\lambda_{max})$, while the area under the unloading curve shown by the blue hatch represent the elastic strain energy density $W_e(\lambda_{max})$. (***C***) Evolution of $W_e(\lambda_{max})$ with cycle *N* for representative samples PA-5 at $\lambda_{max}$=2.34 and 3.14, respectively. The $W_e(\lambda_{max})$ drops greatly at the beginning cycles and reaches a steady state after 3000 cycles. $W_e(\lambda_{max})$ at the 3000$^{th}$ cycle is used to estimate the energy release rate *G* by $G=W_e(\lambda_{max})\times H_0$. (***D***) The ratio of $U_{hys}(\lambda_{max})$ to total work of extension $U_{hys}(\lambda_{max})$ + $W_e(\lambda_{max})$ as a function of cycle *N* for PA-5 at $\lambda_{max}$=2.34 and 3.14, respectively. It also should be noted that $U_{hys}(\lambda_{max})/(U_{hys}(\lambda_{max}) + W_e(\lambda_{max}))$ for $\lambda_{max}$=3.14 is much smaller than for $\lambda_{max}$=2.34, indicating that the reassociation ability of ionic bonds decreases at large $\lambda_{max}$ ($>\lambda_{affine}$).

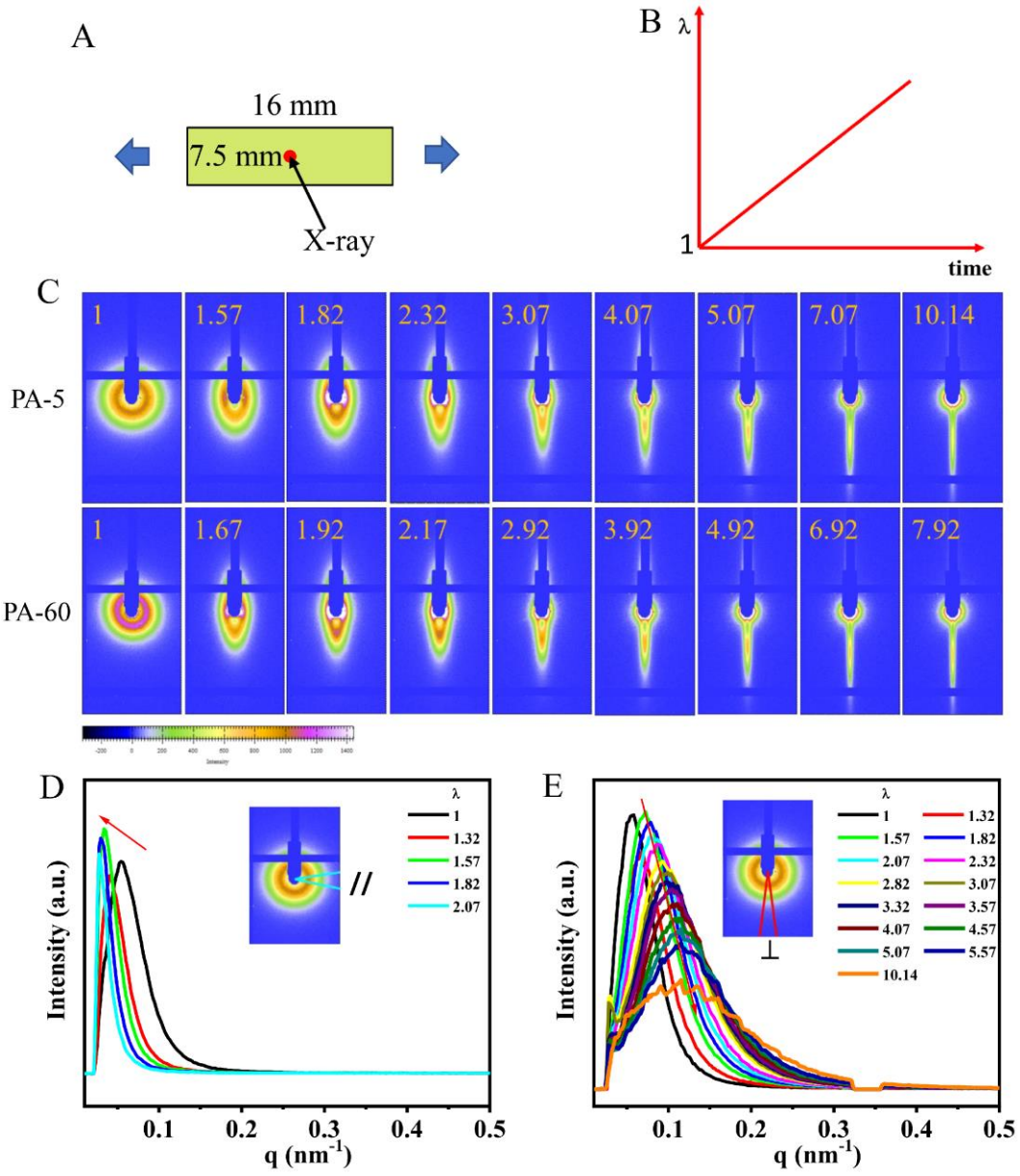


**Fig. S3.**

***In-situ* time-resolved SAXS measurements during tensile test.** (***A***) The illustration of the specimen used in *in-situ* SAXS tests. (***B***) Tensile time profile. The nominal strain rate is 1 $s^{-1}$. (***C***) Evolution of 2D SAXS pattern with λ for representative gels PA-5 and PA-60. (***D*** and ***E***) Evolution of 1D SAXS profiles with λ for PA-5 during tensile tests along the parallel (//) (***D***) and perpendicular (⊥) (***E***) directions. In the parallel direction, the periodic peak shifted to low $q$ with increasing λ and finally beyond the detector range, while the peak shifted to high $q$ in the perpendicular direction. These results demonstrate that the bicontinuous networks are stretched in the tensile direction and compressed in the perpendicular direction. The $q$ at the periodicity peak $q_{max}$ was used to obtain domain spacing ($d$) by $d=2\pi/q_{max}$.

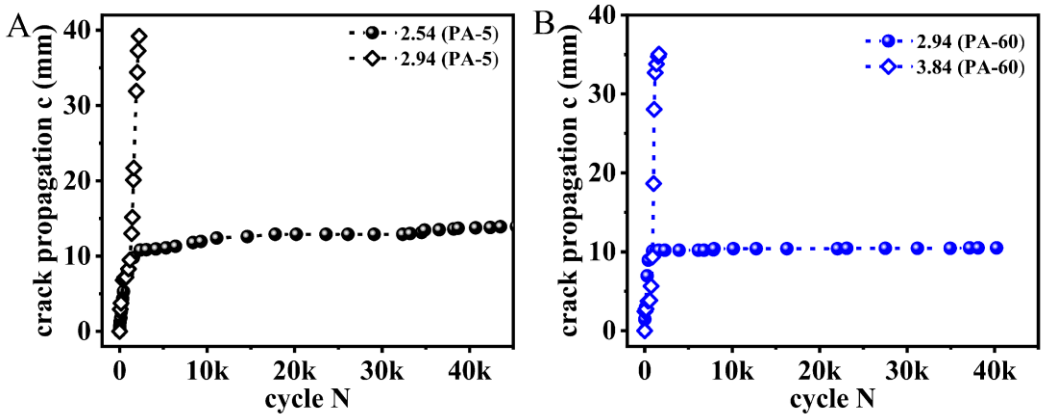


**Fig. S4.**

**Crack propagation length *c* as a function of cycle *N*** at representative elongation ratio $\lambda_{max}$=2.54 ($<\lambda_{affine}$) and $\lambda_{max}$=2.94 ($>\lambda_{affine}$) for PA-5 (***A***), as well as $\lambda_{max}$=2.94 ($<\lambda_{affine}$) and $\lambda_{max}$=3.84 ($>\lambda_{affine}$) for PA-60 (***B***).

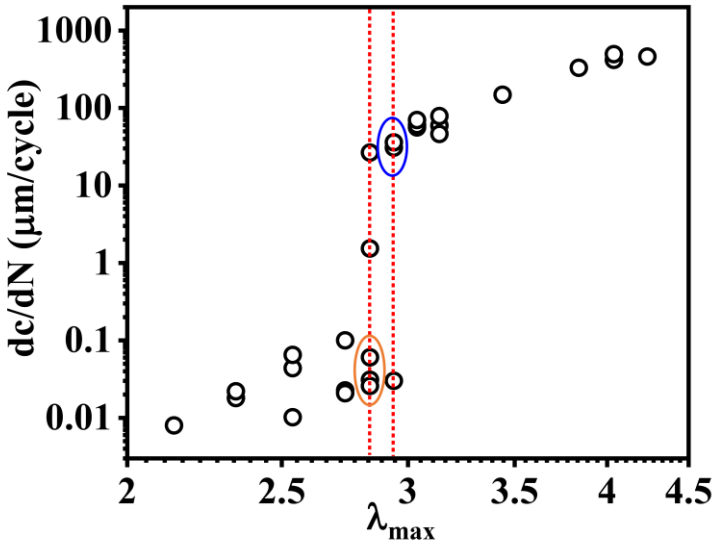


**Fig. S5.**

**The fatigue result for the representative sample PA-5.** We observed a narrow transition regime where both slow and fast crack propagation modes co-exist, as shown by the two dotted vertical lines. We determined the $\lambda_{tran}$ (also $G_{tran}$) as the middle point in this transition regime ($\lambda_{max}$=2.89) and the standard deviation of $\lambda_{tran}$ ($G_{tran}$) as the half width of this transition regime. The $\Delta c/\Delta N$ values at the boundary of the transition regime, $\lambda_{max}$=2.84 and 2.94 in **Fig. 3** ***D***, ***E***, ***F***, are obtained from the statistical average values of the high probability mode at the corresponding $\lambda_{max}$, i.e., the points in orange circle and in blue circle were used to calculate the $\Delta c/\Delta N$ at $\lambda_{max}$=2.84 and 2.94, respectively. This method is also applied to sample PA-30 and sample PA-60.

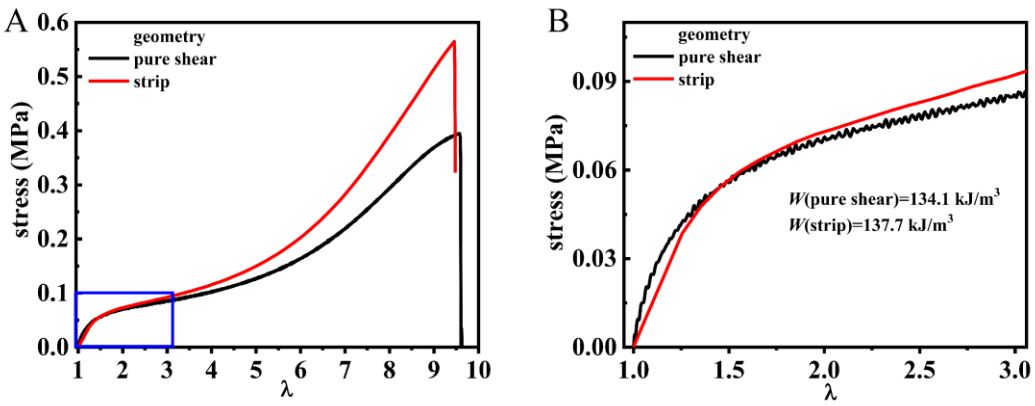


**Fig. S6.**

**Comparison of stress-elongation curves under uniaxial tensile test using sample with the same pure shear geometry in fatigue test (unnotched) and strip geometry in SAXS test.** PA-30 is taken as presentative sample. The nominal strain rate is 1 $s^{-1}$. (***A***) Stress-elongation curves to fracture. The blue rectangle corresponds to the affine deformation regime of hard phase network determined by the SAXS measurement. (***B***) Enlarged affine deformation region. We can see that the differences of stress and work of extension *W* in the affine deformation region between the pure shear geometry and strip geometry are small.

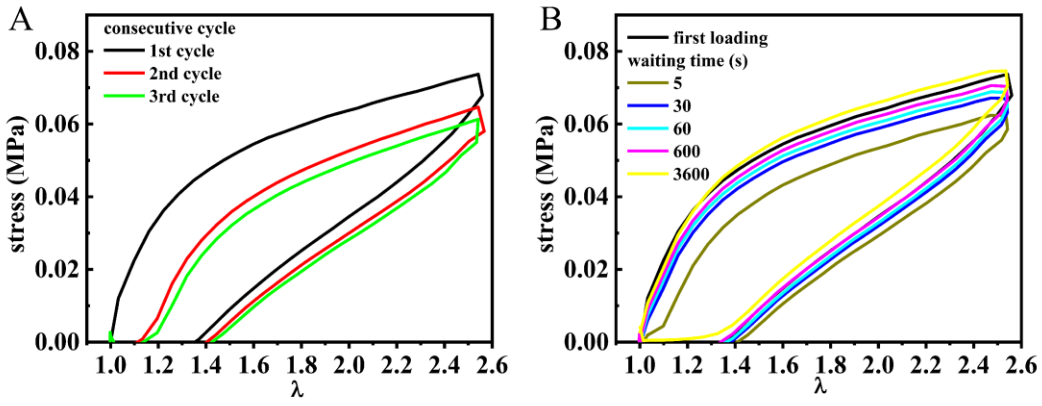


**Fig. S7.**

**Self-recovery behavior of the representative sample PA-30.** (***A***) Stress-stretch ratio curves for the sample subjected to consecutive cyclic tensile for 3 cycles under $\lambda_{max}$=2.54 with strain rate 1 $s^{-1}$. (***B***) Loading-unloading curves of the cyclic tensile test at different waiting times between the first consecutive cyclic tensile and reloading. We can see that residual strain exists after consecutive cyclic tensile. The waiting time for sample recovering to its initial length is about 30 s, but it takes more than 600 s for stress-stretch ratio curve recovering completely (recover to the original rearrangement of ionic pairs).

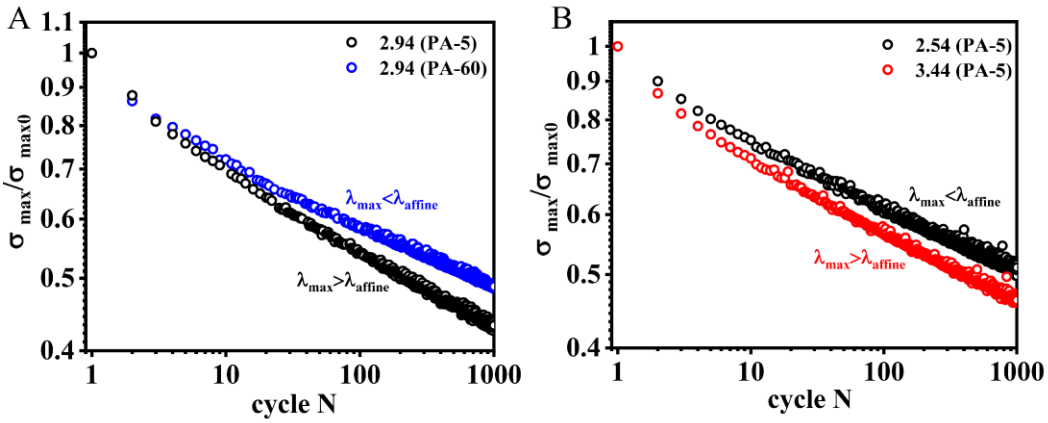


**Fig. S8.**

**Force-carrying ability of unnotched sample under cyclic loading.** (***A***) The change of normalized maximum stress ($\sigma_{max}/\sigma_{max0}$) at $\lambda_{max}$=2.94 with cycle *N* for samples PA-5 ($\lambda_{max}>\lambda_{affine}$) and PA-60 ($\lambda_{max}<\lambda_{affine}$). (***B***) The change of $\sigma_{max}/\sigma_{max0}$ at $\lambda_{max}$=2.54 ($<\lambda_{affine}$) and $\lambda_{max}$=3.44 ($>\lambda_{affine}$) with cycle *N* for sample PA-5. The stress carrying ability becomes weaker with cycle *N* for sample experiencing cyclic loading at $\lambda_{max}>\lambda_{affine}$ compared with at $\lambda_{max}<\lambda_{affine}$, owing to the fracture of hard phase network.

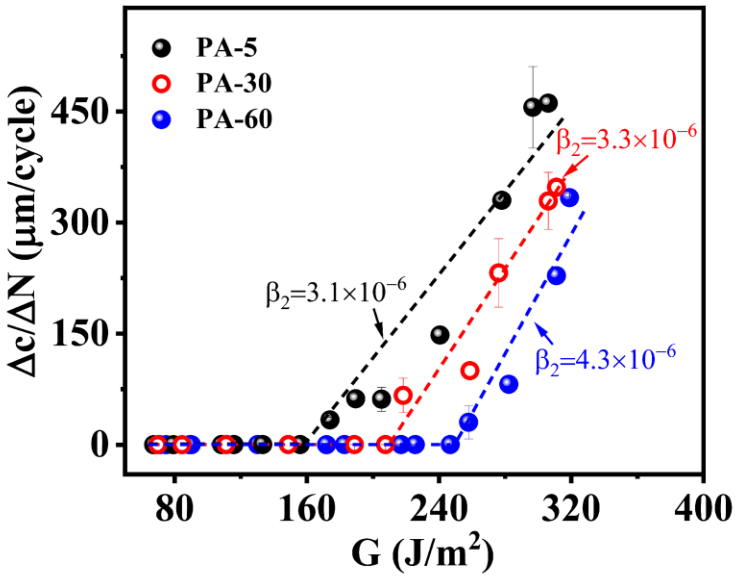


**Fig. S9.**

**Linear plot of Δ*c*/Δ*N* versus *G* in the fast crack propagation regime.** Linear relations are observed, and the slope $\beta_2$ increases slightly with dialysis temperature of the samples, which is related to the increase of phase contrast of the samples. A higher phase contrast, coming from the larger concentration contrast of the hard and soft phase networks, results in sparser chains in soft phase network, which causes a worse fatigue resistance after fracture of hard phase network.

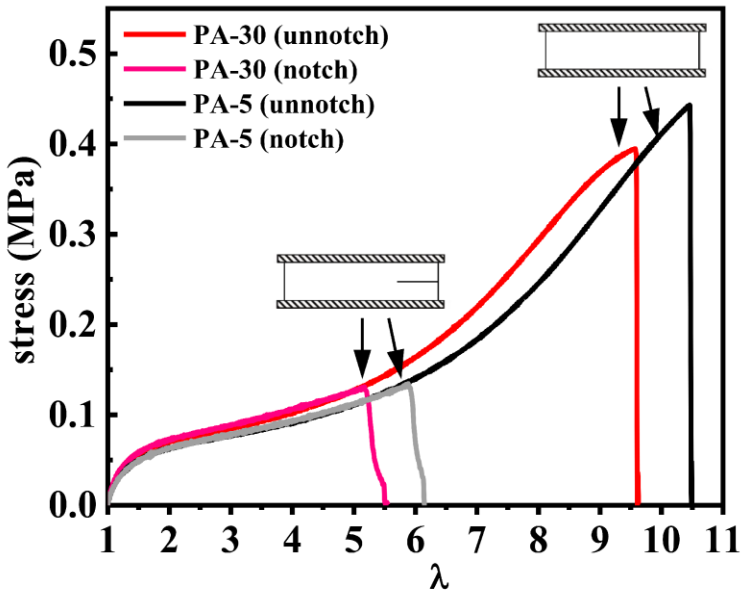


**Fig. S10.**

**Notch sensitivity of PA gels as seen from the tensile behaviors of samples with and without notch in the pure shear geometry.** Although the gels without pre-notch can be extended to a large λ (~10), the gels with pre-notch can only be extended to a much smaller λ (5~6). These results indicate that the gels are notch sensitive, due to rupture of the hard phase network at $\lambda > \lambda_{affine}$. The stress is corrected by the initial effective sample width (i.e. $L_0$=40 mm for notched sample, and $L_0$=50 mm for unnotched sample).

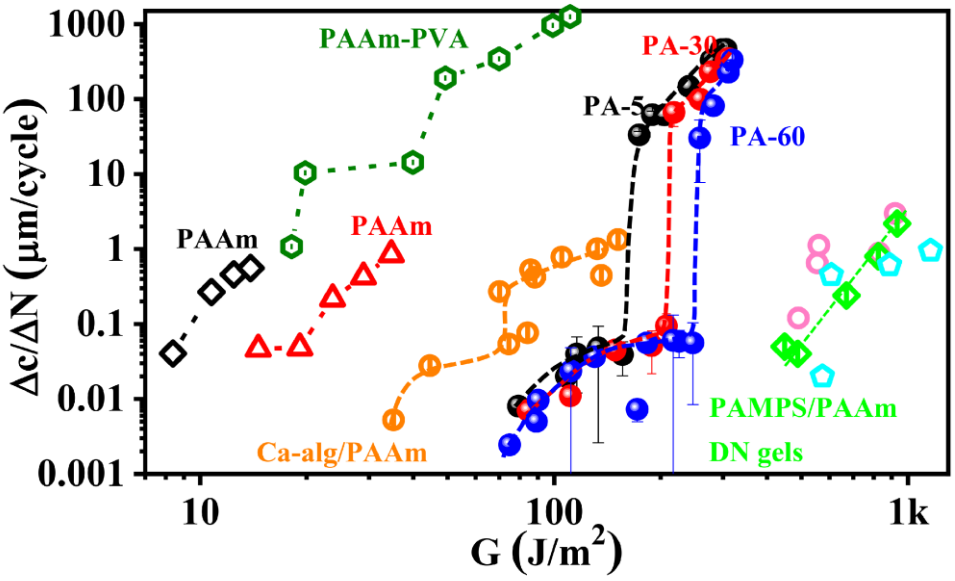


**Fig. S11.**

**Fatigue behaviors of various amorphous hydrogels:** elastic single network PAAm gels (the data is collected from the literature (8)), tough PAMPS/PAAm double network (DN) gels(the data is collected from the literature (9)), tough and self-healing PAAm-PVA gels (the data is collected from the literature (10)) and Ca-alginate/PAAm gels (the data is collected from the literature (11)), as well as PA gels studied in this work.

## SI References


1. Sun TL, *et al.* (2013) Physical hydrogels composed of polyampholytes demonstrate high toughness and viscoelasticity. *Nat. Mater.* 12(10):932.
2. Ihsan AB, *et al.* (2016) Self-healing behaviors of tough polyampholyte hydrogels. *Macromolecules* 49(11):4245-4252.
3. Ihsan AB, *et al.* (2013) A phase diagram of neutral polyampholyte–from solution to tough hydrogel. *J. Mater. Chem. B* 1(36):4555-4562.
4. Lake G & Thomas A (1967) The strength of highly elastic materials. *Proc. R. Soc. London A* 300(1460):108-119.
5. Creton C (2017) 50th anniversary perspective: Networks and gels: Soft but dynamic and tough. *Macromolecules* 50(21):8297-8316.
6. Rivlin R & Thomas AG (1953) Rupture of rubber. I. Characteristic energy for tearing. *J. Polym. Sci.* 10(3):291-318.
7. Long R & Hui C-Y (2016) Fracture toughness of hydrogels: measurement and interpretation. *Soft Matter* 12(39):8069-8086.
8. Zhang E, Bai R, Morelle XP, & Suo Z (2018) Fatigue fracture of nearly elastic hydrogels. *Soft matter* 14(18):3563-3571.
9. Zhang W, *et al.* (2018) Fatigue of double-network hydrogels. *Eng. Fract. Mech.* 187:74-93.
10. Bai R, Yang J, Morelle XP, Yang C, & Suo Z (2018) Fatigue fracture of self-recovery hydrogels. *ACS Macro Lett.* 7(3):312-317.
11. Zhang W, *et al.* (2018) Fracture toughness and fatigue threshold of tough hydrogels. *ACS Macro Lett.* 8(1):17-23.